Available on the CERN CDS information server **CMS PAS SUS-11-004**

CMS Physics Analysis Summary

Contact: cms-pag-conveners-susy@cern.ch 2011/08/30

Search for supersymmetry in all-hadronic events with missing energy

The CMS Collaboration

Abstract

A search for new physics is presented based on an event signature of at least three jets accompanied by large missing transverse momentum, using a data sample corresponding to an integrated luminosity of 1.1 fb^{-1} collected in proton–proton collisions at $\sqrt{s} = 7\,\text{TeV}$ with the CMS detector at the LHC. No excess of events is observed above the expected standard model backgrounds, which are all estimated from the data. Exclusion limits are presented for the constrained minimal supersymmetric extension of the standard model.

1 Introduction

Several theories beyond the standard model (SM) of particle physics address the gauge hierarchy problem and other shortcomings of the SM by introducing a spectrum of new particles that are partners of the SM particles [1–3]. These new particles may include neutral, stable, and weakly interacting particles that are good dark-matter candidates. The identity and properties of the fundamental particle(s) that make up dark matter are two of the most important unsolved problems in particle physics and cosmology. The energy density of dark matter is approximately five times larger than for the normal baryonic matter that corresponds to the luminous portion of the universe. A review on dark matter can be found in Ref. [4].

In many models, dark-matter candidates are stable as a result of a conserved quantity. In supersymmetry (SUSY) this quantity is R parity, and its conservation requires all SUSY particles to be produced in pairs and the lightest SUSY particle (LSP) to be stable. Coloured SUSY particles can be pair-produced copiously at the Large Hadron Collider (LHC). These particles will decay directly into SM particles and an LSP or via intermediate colour-singlet states that ultimately decay into an LSP. The LSP will pass through the detector without interacting, carrying away a substantial amount of energy and creating an imbalance in the measured transverse momentum (p_{T}).

Experiments at the Tevatron [5–7], SPS [8, 9], LEP [10–13], and HERA colliders [14, 15] have performed extensive searches for SUSY and set lower limits on the masses of SUSY particles. At the LHC the CMS Collaboration has previously published limits based on 36 pb^{-1} of data collected in 2010 in the all-hadronic channel. These searches use the α_{T} kinematic variable [16, 17], the *razor* variables [18], and a more generic method based on events in the tails of the missing transverse momentum $\not\!\!H_{\mathrm{T}}$ (defined in Section 3.2) [19]. More recently CMS presented limits based on 1.1 fb^{-1} of the 2011 data using the α_{T} [20] and M_{T2} [21–23] variables. The ATLAS Collaboration also published limits from a missing transverse momentum and multijet search based on the 2010 data [24], and more recently presented updated results based on the 2011 data [25].

In this paper, results are presented from a search for large missing transverse momentum in multijet events produced in pp collisions at a centre-of-mass-energy of 7 TeV, using a data sample collected with the CMS detector at the LHC in 2011, corresponding to an integrated luminosity of 1.1 fb^{-1}. This search follows a strategy similar to the one used in [19]. The results of the search are presented in the context of the constrained minimal supersymmetric extension of the standard model (CMSSM) [26–28].

The main backgrounds in this analysis are: an irreducible background from Z+jets events, with the Z boson decaying to $\nu\bar{\nu}$, denoted as $\mathrm{Z}(\nu\bar{\nu})$+jets; W+jets and $\mathrm{t\bar{t}}$ events, with either the directly-produced W boson or one of the W bosons from the top-quark decaying directly or via a τ to an e or μ that is lost, or to a τ that decays hadronically. In all these cases, one or more neutrinos provide a source of genuine missing transverse momentum. The third background category is QCD multijet events with large missing transverse momentum from leptonic decays of heavy-flavour hadrons inside the jets, jet energy mismeasurement, or instrumental noise and non-functioning detector components. All these backgrounds are directly determined from the data in this search.

This paper is organized as follows. The CMS detector and event reconstruction are described in Section 2. In Section 3, the event selection criteria are presented. In Section 4, the irreducible $\mathrm{Z}(\nu\bar{\nu})$+jets background is estimated from γ+jets events. The background from W+jets and $\mathrm{t\bar{t}}$ where a lepton is either lost or is a hadronically decaying tau lepton is estimated from μ+jets

events by ignoring the muon or replacing it with a simulation of a hadronically-decaying tau jet, as discussed in Section 5. The QCD multijet kinematics are predicted using measured jet resolution functions to smear events obtained by a procedure that produces well-balanced events out of inclusive multijet data, as discussed in Section 6. In Section 7, the interpretation of the observed data is presented.

2 The CMS Detector and Event Reconstruction

The central feature of the CMS apparatus is a superconducting solenoid 13m in length and 6m in diameter which provides an axial magnetic field of 3.8 T. The bore of the solenoid is instrumented with various particle detection systems. The iron return yoke outside the solenoid is in turn instrumented with gas detectors which are used to identify muons. Charged particle trajectories are measured by the silicon pixel and strip tracker, covering $0 < \phi < 2\pi$ in azimuth and $|\eta| < 2.5$, where the pseudorapidity η is defined as $\eta = -\log\tan(\theta/2)$, with θ being the polar angle of the trajectory of the particle with respect to the counterclockwise beam direction. A lead-tungstate crystal electromagnetic calorimeter (ECAL) and a brass/scintillator hadronic calorimeter (HCAL) surround the tracking volume and cover the region $|\eta| < 3$. Quartz/steel forward hadron calorimeters extend the coverage to $|\eta| \leq 5$. The detector is nearly hermetic, allowing for energy balance measurements in the plane transverse to the beam direction. A detailed description of the CMS detector can be found in Ref. [29].

All physics objects are reconstructed using the particle-flow algorithm [30]. This algorithm identifies and reconstructs, individually, all types of particles produced in the collision, namely charged hadrons, photons, neutral hadrons, muons, and electrons, by combining the information from the tracking system, the calorimeters, and the muon system. These reconstructed particles are fully calibrated. All these particles are clustered into jets using the anti-k_T algorithm with parameter $D = 0.5$ [31]. Jets are corrected using factors derived from simulation, and, for jets in data, an additional residual energy correction derived from the data is applied [32]. In addition, jets are corrected for energies coming from additional pileup pp collisions using the fastjet approach [33, 34] that relies on the jet area calculation and an event transverse energy density measurement.

3 Sample Selection

3.1 Selection and cleaning of the data sample

This analysis is performed using a data sample corresponding to an integrated luminosity of 1.1 fb^{-1} collected from March to June 2011. These data are collected by trigger paths based on $H_{\text{T}}^{\text{trigger}}$ and, for the majority of the data, also on $\not{H}_{\text{T}}^{\text{trigger}}$. $H_{\text{T}}^{\text{trigger}}$ is defined as the scalar sum of jet transverse momenta, based on calorimetric information only, with the corrected $p_{\text{T}} > 40\,\text{GeV}$ and $|\eta| < 3$, and $\not{H}_{\text{T}}^{\text{trigger}}$ as the magnitude of the negative vector sum of transverse momenta of jets with the corrected $p_{\text{T}} > 30\,\text{GeV}$ and $|\eta| < 3$. In order to keep the trigger rate acceptable during the course of the data taking, the thresholds on $H_{\text{T}}^{\text{trigger}}$ and $\not{H}_{\text{T}}^{\text{trigger}}$ were changed between 160 and 260 and between 60 and 90 GeV, respectively. The trigger efficiency as a function of the offline particle-flow based H_{T}, defined in Section 3.2, has been measured in data collected with a more inclusive H_{T} trigger. The set of H_{T} and $\not{H}_{\text{T}}$ triggers are fully efficient for an offline H_{T} above 350 GeV and $\not{H}_{\text{T}}$ above 200 GeV.

The cleaning of fake $\not{H}_{\text{T}}$ due to instrumental effects, particles from non-collision sources, and reconstruction failure is the key element in this search. Various sources of noise in the hadron [35]

and electromagnetic calorimeters are rejected. Beam-related background events and displaced satellite collisions are removed by requiring a well-reconstructed primary vertex, applying a beam-halo veto [36], asking for a significant fraction of tracks in the event to pass high quality criteria, and requiring the scalar sum of the transverse momenta of tracks associated to the primary vertex to be greater than 10% of the scalar sum of transverse momenta of all jets within the tracker acceptance. Finally, events are rejected in which a significant amount of energy is determined to be lost in $\sim 1\%$ of crystals in the ECAL masked during reconstruction [36, 37]. Such losses are identified either using the energy measured through a parallel readout path used for the online trigger, or by measuring the energy deposited around masked crystals for which this parallel readout path is nonfunctional.

3.2 Baseline and search event selections

The search selection starts from a loose validation region, which is referred to as the baseline selection. On this baseline selection tighter selection criteria are applied to define the search selections, as described further in this section. The search selections were chosen based on the expected signal efficiency in the CMSSM plane, and the amount of SM background. The baseline selection requirements after trigger are:

- At least three jets with $p_{\mathrm{T}} > 50\,\mathrm{GeV}$ and $|\eta| < 2.5$.
- $H_{\mathrm{T}} > 350\,\mathrm{GeV}$, with H_{T} defined as the scalar sum of the p_{T}s of all the jets with $p_{\mathrm{T}} > 50\,\mathrm{GeV}$ and $|\eta| < 2.5$.
- $\not{H}_{\mathrm{T}} > 200\,\mathrm{GeV}$, with $\not{H}_{\mathrm{T}}$ defined as the magnitude of the negative vectorial sum of the p_{T}s of the jets having, in this case, $p_{\mathrm{T}} > 30\,\mathrm{GeV}$ and $|\eta| < 5$. The majority of QCD events in the MHT tail are removed with this requirement.
- $|\Delta\phi(J_n, \not{H}_{\mathrm{T}})| > 0.5$ (rad), $n = 1, 2$ and $|\Delta\phi(J_3, \not{H}_{\mathrm{T}})| > 0.3$ (rad), vetoing events in which $\not{H}_{\mathrm{T}}$ is aligned in the transverse plane along one of the three leading jets. This requirement rejects most of the QCD multijet events in which a single mismeasured jet yields a high $\not{H}_{\mathrm{T}}$.
- Veto on isolated muons and electrons. A loose lepton definition is employed to reject the leptonic final states of $\mathrm{t\bar{t}}$ and W/Z+jets events. Muons and electrons are required to have $p_{\mathrm{T}} \geq 10$ GeV. Muons are required to have $|\eta| < 2.4$, whereas electrons should have $|\eta| < 2.5$, excluding the transition region $1.444 < |\eta| < 1.566$. Their quality and isolation requirements are the same as those used in the 2010 data analysis [19].

Three search regions were chosen based on H_{T} and $\not{H}_{\mathrm{T}}$:

- The *medium-H_{T} & $\not{H}_T$* search region tightens the baseline cuts by requiring both $H_{\mathrm{T}} > 500$ and $\not{H}_{\mathrm{T}} > 350\,\mathrm{GeV}$ requirements.
- The *high-H_{T}* search region tightens the baseline H_{T} cut with an $H_{\mathrm{T}} > 800\,\mathrm{GeV}$ requirement, to improve sensitivity to higher object multiplicities like those expected in the case of long cascade decays. Such cascades lead to more energy being transferred to visible particles rather than to the dark-matter candidates.
- The *high-$\not{H}_T$* search region tightens the *high-H_{T}* selection by requiring $\not{H}_{\mathrm{T}} > 500\,\mathrm{GeV}$, resulting in high background rejection.

3.3 Comparisons of data and simulation

Several Monte-Carlo (MC) samples produced with a detailed Geant-based [38] CMS detector simulation were used. Samples of QCD multijet, $\mathrm{t\bar{t}}$, W, Z and γ+jets were generated with the

Table 1: Event yield in data and simulated samples. The latter are normalized to an integrated luminosity of 1.1 fb^{-1}.

	Baseline	Baseline $\geq$ 3jets	Baseline $\geq$ 3jets $\Delta\phi$ cuts	Baseline $\geq$ 3jets $\Delta\phi$ cuts e/μ veto	Medium	High H_T	High $\not{H}_T$
Data	6377	3408	1640	986	78	70	3
Sum SM MC	6406	3227	1709	987	95	83	7.5
QCD multijet (PYTHIA)	1143	549	11.4	11.3	0.3	6.9	0.0
Z($\nu\bar{\nu}$)+jets (MG)	1370	481	387	386	46.3	29	4.2
W($\ell\nu$)+jets (MG)	2963	1365	784	346	37.5	28	2.9
$t\bar{t}$ (MG)	930	832	527	244	11.3	18	0.4
LM4 (PYTHIA)	1477	1179	942	742	318	304	54

PYTHIA6 [39] and MADGRAPH [40] generators. For the $t\bar{t}$ background an approximate next-to-next-to-leading-order (NNLO) cross section from [41] is used, while for the W($\ell\nu$)+jets and Z($\nu\bar{\nu}$)+jets backgrounds the NNLO calculation with FEWZ [42] is used. The LM4 CMSSM point [43] defined with parameters $m_0 = 210\,\text{GeV}$, $m_{1/2} = 285\,\text{GeV}$, $A_0 = 0$, $\tan\beta = 10$, and sign(μ) > 0, is used as a benchmark for new physics. This point has the next-to-leading-order (NLO) cross section of $\sigma = 2.5\,\text{pb}$, as calculated with PROSPINO [44].

The event yield in data and MC simulated samples after the event selection is summarized in Table 1, where event yields for MC simulation correspond to an integrated luminosity of 1.1 fb^{-1}. The H_T, $\not{H}_T$, and $M_{\text{eff}}(= H_T + \not{H}_T)$ distributions are compared between data and MC simulation in Fig. 1 after the baseline selection. However, these simulation predictions are not used further in the analysis. In the following sections all the backgrounds to this search are estimated using the collider data directly.

4 Invisible Z Background Estimation

The associated production of a Z boson and jets followed by the decay of the Z boson into neutrinos constitutes an irreducible background. To estimate this background from the data, two methods are pursued; the primary method for this analysis uses γ+jets, whilst the other method using Z($\ell^+\ell^-$)+jets provides an important cross-check.

The method using Z($\ell^+\ell^-$)+jets events is the most straightforward one. By interpreting the pair of leptons as missing momentum the topology of the $Z \to \nu\bar{\nu}$ process can be reproduced and all jet-related selection criteria can be directly applied. To predict the number of $Z \to \nu\bar{\nu}$ events, the measured number of Z($\ell^+\ell^-$)+jets events are corrected for the acceptance, efficiencies and the branching fraction ratio of $R(Z \to \nu\bar{\nu}/Z \to \ell^+\ell^-) = 5.95$. The disadvantage of this method is that only a small number of $Z \to \ell^+\ell^-$ events survive the selection criteria used to define the search regions. This method is used to verify the predicted $Z \to \nu\bar{\nu}$ rates for the higher statistics baseline selection and the results are found to be in reasonable agreement with the prediction from γ+jets, described below.

The primary method used for this analysis exploits the electroweak correspondence between the Z boson and photon at high boson p_T. The photon production is within 20% of inclusive Z production, and the cross section ratio depends mostly on the electroweak rather than hadronic characteristics of the events. Therefore this ratio can provide a robust prediction of the missing momentum spectrum for invisible Z bosons at high p_T. Being consistent with and more precise

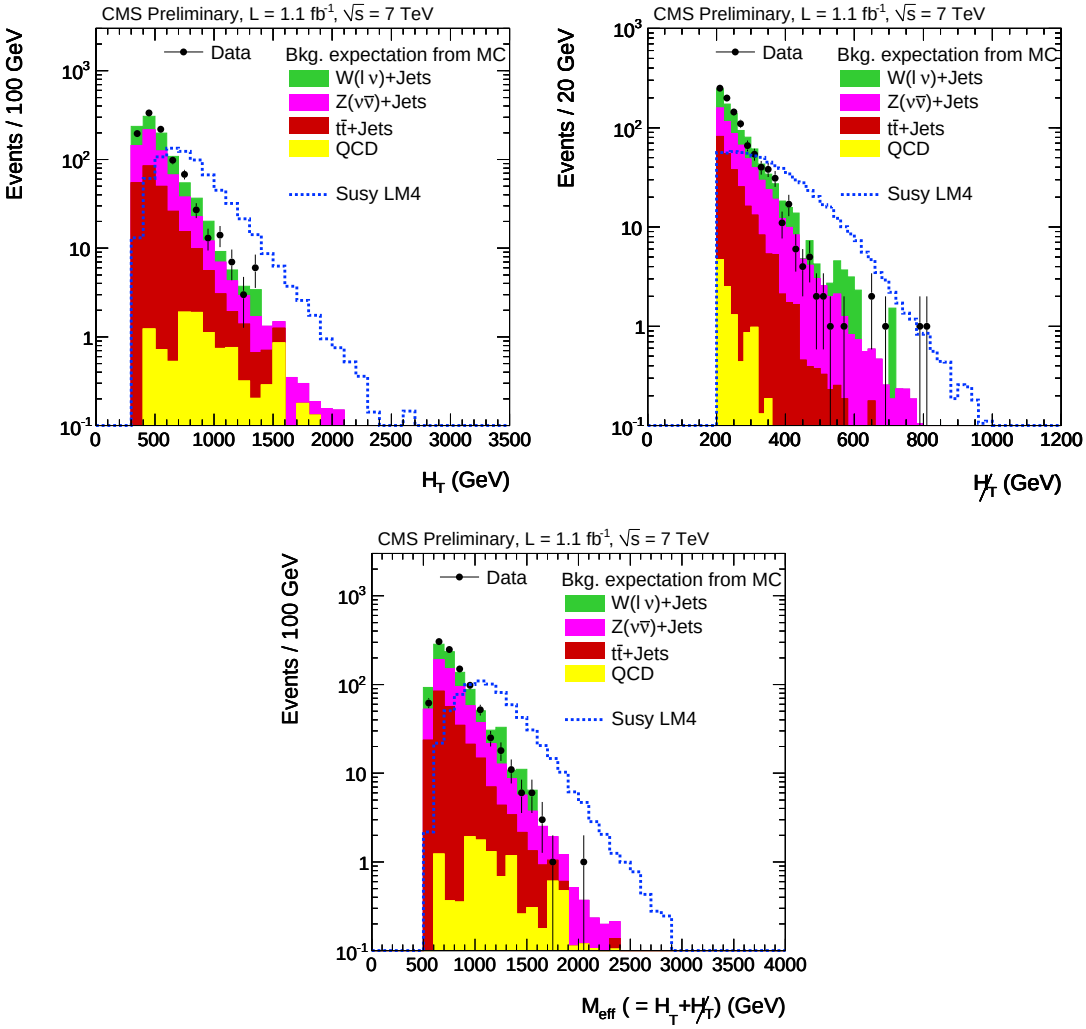

Figure 1: H_{T}, $\not{H}_{\mathrm{T}}$, and effective mass (M_{eff} defined as sum of H_{T} and $\not{H}_{\mathrm{T}}$) distributions for the data and MC simulation samples with all baseline selection cuts applied.

than the $Z(\ell^+\ell^-)$+jets results, the γ+jets results are used as the primary measurement of the $Z \to \nu\bar{\nu}$ background.

4.1 Estimation from γ+jets

The γ and Z boson arise in the electroweak theory after symmetry breaking as neutral eigenstates coupling to the electromagnetic and weak interactions respectively. Their production properties are very different at energies below or of the order of the Z boson mass, but at higher energies they exhibit similar characteristics, apart from electroweak coupling differences and asymptotically vanishing residual mass effects. One important distinction between Z and γ production arises from the breakdown of the leading-order calculation of γ+jets production for small-angle or vanishing-energy emission of the γ relative to the parent quark in the absence of a mass to regularize the resulting divergences. This is mitigated by imposing isolation requirements on the selected γ sample.

The prediction of the $Z \to \nu\bar{\nu}$ background using γ+jets production starts with the selection of a highly pure γ+jet control sample. The data are collected using single-photon triggers, which were measured to be fully efficient for events passing the baseline selection. In the offline selection photon candidates are distinguished from electrons with a veto on the presence of a track segment in the pixel detector. Photons from QCD multijet events are suppressed by requiring isolation in the tracker and calorimeters and with a requirement on the shower shape in the η coordinate [45]. Finally, to be able to predict the invisible Z background from the photon sample, the jet-related quantities in the analysis event selection are restricted to the photon recoil.

A comparison of the shapes of the H_T and $\not{H}_T$ in photon events is shown in Fig. 2. The MC has been scaled to match the normalization of the data. The shapes agree well.

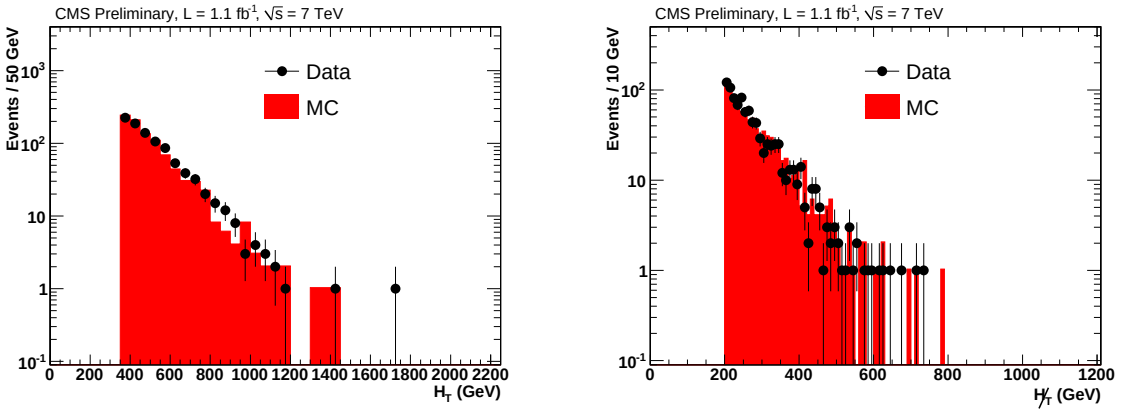

Figure 2: H_T (left) and $\not{H}_T$ (right) distributions after the baseline selection for photon data and MC.

For the derivation of the phenomenological γ-Z correction factor, simulated γ+jets and $Z \to \nu\bar{\nu}$ MADGRAPH samples are used.

Before predicting the invisible Z background from the selected γ+jets sample, the backgrounds to the direct photons need to be subtracted. This subtraction is performed after imposing isolation requirements, which strongly suppress the background from QCD multijet events. The contribution of fragmentation photons, which do not have a counterpart in the massive Z boson production, is estimated from NLO JETPHOX [46] calculations to be $(5 \pm 1)\%$ [47] in the se-

lected photon sample. A second background arises from isolated neutral pions and η mesons decaying to pairs of so-called secondary photons. For hard mesons, these photon pairs get sufficiently collimated to be reconstructed as a single photon. The fraction of QCD jets mimicking a photon is measured as a function of p_T and η using an isolation template [48]. Using these results, the purity of the photon sample passing the baseline selection is estimated to be $(92.9 \pm 7.8)\%$. The fraction of electrons failing the track match and thus contributing to the photon sample is negligible.

The selected γ+jets control sample requires corrections after background subtraction to obtain a prediction for the number of $Z(\nu\bar{\nu})$+jets events passing the search selections. The above described photon selection and isolation are applied on the MC-simulated samples to estimate this correction factor. The phenomenological correction factor is separated into three parts; the ratio of event yields at generator-level, the geometric acceptance, and the efficiency of selecting reconstructed photons. The generator-level event yield ratio is flat across H_T and $\not{H}_T$ as determined using a high statistics MC sample.Therefore the ratio obtained in the baseline selection region is used for all the search regions. The individual acceptances and efficiencies are computed specifically for each search region. The correction factors for the baseline, medium, high-H_T, and high-$\not{H}_T$ selection are estimated to be respectively 0.47 ± 0.07, 0.48 ± 0.07, 0.57 ± 0.08 and 0.51 ± 0.08, where the uncertainties are statistical only. Other uncertainties arise from the acceptance, (5% [17]), and from the phenomenological factor itself. The latter theoretical uncertainty is estimated from a comparison of leading to next-to-leading-order calculations of the ratio of γ and Z production with two jets [49]. This dedicated calculation was performed in the 2010 data analysis for the different selections in the analysis adapted to only two jets. The addition of an extra jet was not expected to induce a significant effect. Ref. [50] shows the ratio of predicted leading-order cross-sections varying as a function of boson p_T on the order of 15%; we therefore conservatively double the uncertainty used in the previous analysis [19] to 20%. This 20 % theoretical uncertainty on the Z/γ cross-section ratio is taken as a uniformly distributed systematic uncertainty with a standard deviation of 12 %.

The remaining correction factors to the photon yield involve experimental aspects of the photon selection. Firstly, the photon reconstruction inefficiency, due to the possible presence of a pixel seed from early photon conversions or from coincidences between photons and tracks, is estimated in [47] to be $(3.5 \pm 1.4)\%$. This inefficiency is taken into account by the γ-Z correction factor above, but the uncertainty is reported here separately. Secondly, the photon identification and isolation efficiency, which enters the phenomenological correspondence factor with an estimate from simulation, needs to be corrected for the difference between data and simulation. Using the results obtained in a tag-and-probe study on $Z \to e^+e^-$ events, the needed correction was determined to be $0.98 \pm 3.0\%$.

In Table 2 the full list of corrections is summarized, along with the corresponding systematic uncertainties, for the baseline and search selections. The results for the $Z(\nu\bar{\nu})$+jets prediction from the γ+jets data sample are summarized in Table 3.

5 W and Top Background Estimation

The muon and electron vetoes, described in Section 3.2, aim to suppress SM events with an isolated lepton. However, events from $t\bar{t}$ and W+jets production are not rejected by this lepton veto if a lepton falls out of geometric or kinematical acceptance, or is not identified or not isolated, or if a τ lepton decays hadronically. In this section two data-driven methods are presented to estimate these two components of the $t\bar{t}$ and W+jets backgrounds. The first method uses a μ+jets control sample and corrects for lepton (in)efficiencies, in order to estimate the

Table 2: Overview of all correction factors and corresponding systematic uncertainties.

	Baseline	Medium	High H_T	High $\not{H}_T$
Fragmentation	0.95±1 %	0.95±1 %	0.95±1 %	0.95±1 %
Photon purity	0.93±7.8 %	0.99±4.6 %	0.94±7.1 %	1.00±4.5 %
Photon mistag	1.00±1.4 %	1.00±1.4 %	1.00±1.4 %	1.00±1.4 %
±scale	±12 %	±12 %	±12 %	±12 %
Z/γ correction±acceptance	0.47±5 %	0.48±5 %	0.57±5 %	0.51±5 %
±MC stat	±14.25 %	±14.28 %	±14.25 %	±15.66 %
ID data/MC ratio	0.98±3 %	0.98±3 %	0.98±3 %	0.98±3 %
Total correction	0.40±21.0 %	0.47±20.1 %	0.57±20.9 %	0.51±20.8 %

Table 3: The $Z \to \nu\bar{\nu}$ background predicted for each of the selections with the statistical and systematic uncertainties. The prediction corresponds to 1.1 fb^{-1}.

	Baseline	Medium	High H_T	High $\not{H}_T$
Prediction	376 ±12 ±79	42.6 ±4.4 ±8.9	24.9 ±3.5 ±5.2	2.4 ±1.1 ±0.5

orthogonal set of events that fail the lepton identification or isolation, and is referred to as the lost-lepton background. The other method predicts the hadronic tau background from a similar μ+jets control sample by substituting the muon with a τ jet. Both methods predict the combined $t\bar{t}$ and W+jets background.

5.1 The lost-lepton background estimation

The contribution of the $t\bar{t}$ and W+jets events, where the W boson decays into a muon or an electron directly or through a τ lepton and are not rejected by the explicit lepton veto discussed in Section 3.2, is measured using a muon control sample. This control sample is selected by applying the search cuts except for the muon veto and requiring exactly one well-identified and well-isolated muon. In this muon control sample, the transverse mass $m_T = \sqrt{2p_T^{\mu} \not{E}_T(1-\cos(\Delta\phi))}$ is required to be less than 100 GeV in order to suppress possible signal contamination. The $\not{E}_T$ in the above formula is the missing transverse energy, and $\Delta\phi$ represents the distance in ϕ between the $\not{E}_T$ and the muon. More than 97% of this sample arises from $t\bar{t}$ and W+jets events. Events in the isolated muon control sample (CS) are weighted according to the lepton isolation efficiency ϵ_{ISO} in order to model the non-isolated (but identified) leptons (electron or muon separately) in the signal region (!ISO$^{e,\mu}$) according to

$$!\mathrm{ISO}^{e,\mu} = \mathrm{CS} \cdot \frac{1-\epsilon_{\mathrm{ISO}}^{e,\mu}}{\epsilon_{\mathrm{ISO}}^{\mu}} \cdot \frac{\epsilon_{\mathrm{ID}}^{e,\mu}}{\epsilon_{\mathrm{ID}}^{\mu}} \cdot \frac{\epsilon_{\mathrm{Acc}}^{e,\mu}}{\epsilon_{\mathrm{Acc}}^{\mu}}. \quad (1)$$

To model the sample containing non-identified electron or muons in the signal region (!ID$^{e,\mu}$), the control sample is weighted as

$$!\mathrm{ID}^{e,\mu} = \mathrm{CS} \cdot \frac{1}{\epsilon_{\mathrm{ISO}}^{\mu}} \cdot \frac{1-\epsilon_{\mathrm{ID}}^{e,\mu}}{\epsilon_{\mathrm{ID}}^{\mu}} \cdot \frac{\epsilon_{\mathrm{Acc}}^{e,\mu}}{\epsilon_{\mathrm{Acc}}^{\mu}}, \quad (2)$$

where $\epsilon_{\mathrm{ID}}^{e,\mu}$ is the electron (muon) identification efficiency and $\epsilon_{\mathrm{Acc}}^{e,\mu}$ is the electron (muon) acceptance.

The lepton isolation efficiency is measured as a function of lepton p_T relative to the nearest jet and the angular distance ΔR between the lepton and the nearest jet from data Z events

using a tag-and-probe method in order to account for the kinematic differences between Z+jets events and the $t\bar{t}$ and W+jets events. The lepton identification efficiency is parametrized in p_T and lepton pseudo-rapidity η. This parametrization still leaves a small dependence on the kinematic differences between Z+jets and $t\bar{t}$/W+jets events, and leads to an underprediction of the non-reconstructed leptons. The difference between the uncorrected prediction and the background has been studied using simulated events and has been found to be smaller than 10%. The data prediction is corrected for this underprediction, and the size of the correction is taken as a systematic uncertainty.

Leptons can be out of acceptance when the transverse momentum is too small or the leptons are emitted in the forward region. Especially leptons from leptonic tau-decays tend to have low momentum, and the additional neutrinos in the event contribute to its $\not{H}_T$. The average ratio R_{Accept} of events with leptons out of acceptance to events within acceptance is estimated using Monte Carlo simulation. The same data control sample described above, weighted by $R_{\text{Accept}}/(\epsilon_{\text{ISO}} \cdot \epsilon_{\text{ID}})$ to correct for the isolation and identification efficiencies of the control sample, is used to model the non-accepted lepton background.

This procedure is tested on simulated $t\bar{t}$ and W+jets events. The result of the comparison is shown in Fig. 3 as a function of $\not{H}_T$ and H_T. The estimate and the MC truth agree within the uncertainties. The underprediction discussed above of about 7% is used as a correction for the prediction on data. The final prediction is obtained by applying this method to the muon control sample collected using the same H_T trigger as for the search, and is presented in Table 4 and Fig. 4.

Table 4: The lost-lepton background predicted for each of the selections with the statistical and systematic uncertainties. The prediction corresponds to 1.1 fb^{-1}.

	Baseline			Medium			High H_T			high $\not{H}_T$		
Prediction	244	± 20	$^{+30}_{-31}$	12.7	± 3.3	± 1.5	22.5	± 6.7	$^{+3.0}_{-3.1}$	0.8	± 0.8	± 0.1

Except for the baseline selection the dominant uncertainties on the lost-lepton prediction arise from the statistical uncertainties of the control sample and the statistical uncertainties of the Z sample from which the lepton efficiencies were determined. Other systematic uncertainties are related to remaining kinematic differences between the control and signal regions that are not completely absorbed in the lepton efficiency parametrization. A conservative systematic uncertainty of 3% was assigned to take into account any residual presence of QCD, Z or di-boson events in the control sample. A summary of the uncertainties together with their size for the baseline selection can be found in Table 5

5.2 Hadronic τ background estimation

Hadronically decaying tau (τ_h) leptons constitute an important second component of the W and $t\bar{t}$ background to this search. In this section a method is presented which is used to estimate the hadronic-τ background from a μ+jets control sample, mainly composed of W($\mu\nu$)+jets and $t\bar{t}$($\mu\nu$)+jets events. This muon control sample is selected from data collected with single muon triggers, by requiring exactly one muon with $p_T > 20\,\text{GeV}$ and $|\eta| < 2.1$. Since the muon is replaced by a τ jet in this prediction method, only two jets are required in this case instead of three.

Jets from τ leptons are characterized by a low multiplicity of particles, typically a few pions and neutrinos. The fraction of visible energy can be described by a response template, obtained from simulation by matching reconstructed jets with generated τ leptons and determining the

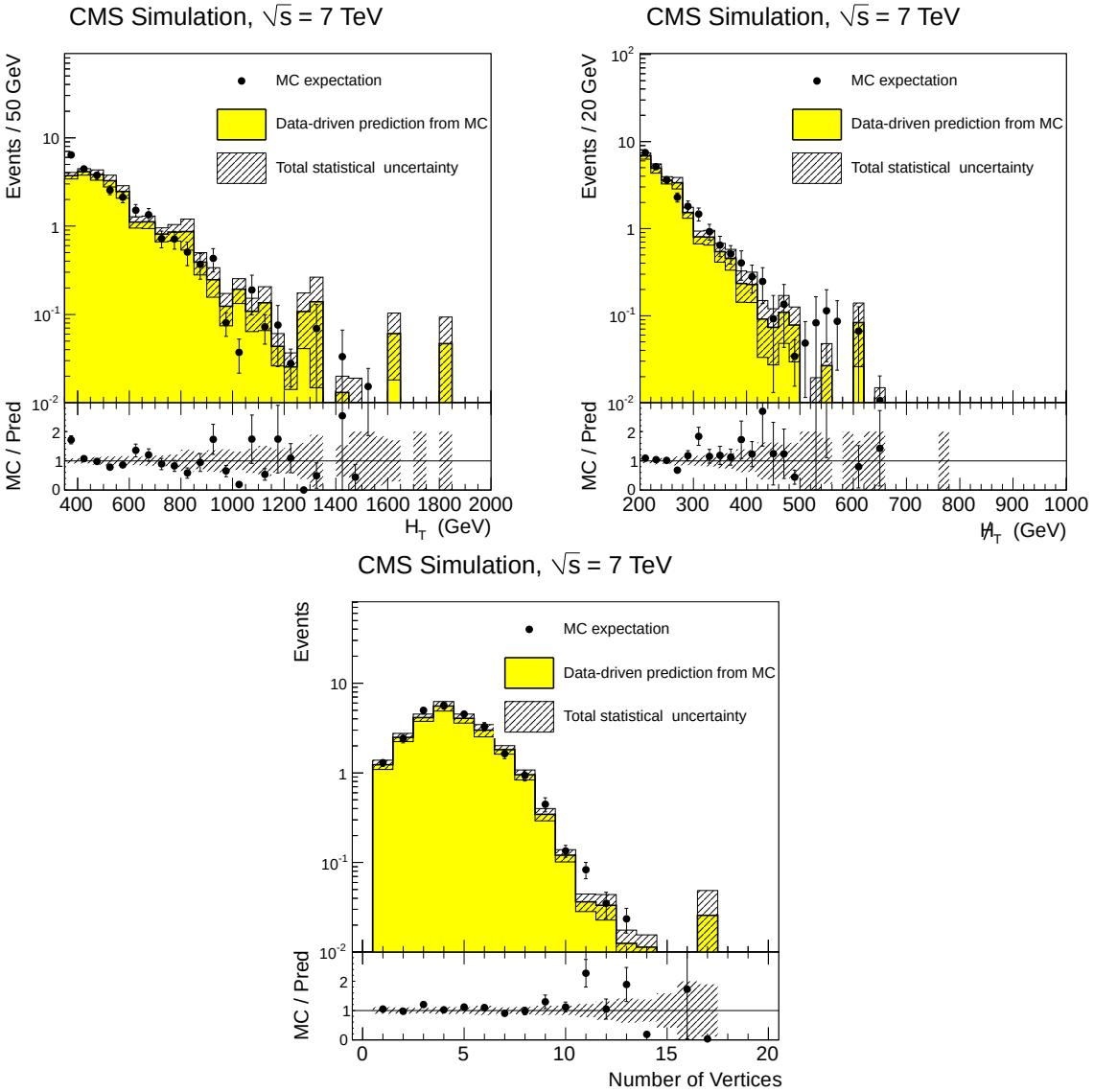

Figure 3: The closure test of the method for the lost-lepton background prediction. The lost-lepton background prediction obtained from MC simulated events using the data-driven method compared to MC $t\bar{t}$ and W+jets expectation. The uncertainty band relates to the total statistical uncertainty of the prediction, i.e. from the control sample and the efficiency measurement. The systematic uncertainties are not included. The shown variables are H_T (top left), $\not{H}_T$ (top right), and the number of primary vertices (bottom). The ratio of the data-driven prediction from MC to the MC expectation is also shown.

Table 5: Systematic uncertainties (in the number of events) of the lost-lepton background prediction.

Source	Systematic Uncertainties
Statistics of control-sample	-19.8 $+19.8$
Iso- & id- efficiencies (statistical)	-10.2 $+10.2$
Differences $t\bar{t}$, W, Z-samples	-24.4 $+24.4$
and kinematic in control vs. signal region	
SM background in control-region	-7.3 $+0$
MC use for acceptance calculation	-9.5 $+9.5$
Transverse W-mass-cut	-10.5 $+10.5$
Total, combined uncertainty	-36.7 $+35.9$

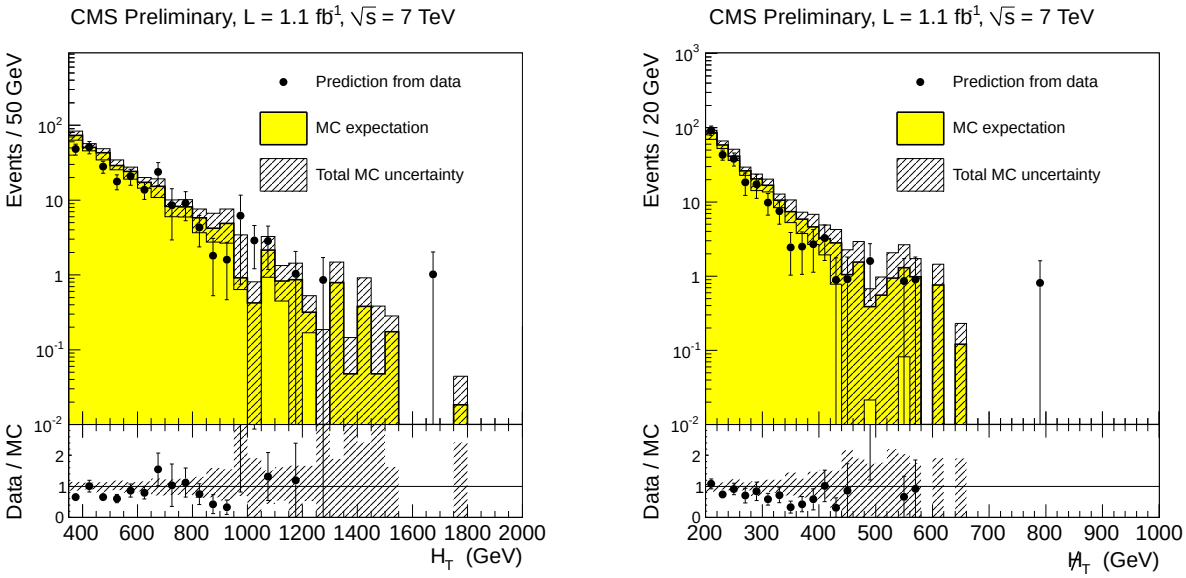

Figure 4: Predictions of the lost-lepton background using the muon control sample from data for H_T (left) and $\not{H}_T$ (right) compared to MC $t\bar{t}$ and W+jets expectation. The ratio of the prediction from data to the MC expectation is also shown.

ratio of the reconstructed τ-jet and the simulated τ-lepton p_T.

The hadronic quantities of events in the muon control sample correspond to the hadronic-τ background except that they miss the visible energy of the τ jet in the detector. To account for this difference, the muon in events in the control sample is replaced by a τ jet, and H_T and $\not{H}_T$ are recalculated taking into account this extra jet. Selection cuts are applied to these modified events to obtain the hadronic-τ background. The τ-jet momentum is obtained by scaling the muon momentum with a factor obtained from sampling the τ energy response template. In order to probe the full template this procedure is repeated multiple times for each event.

Various additional differences need to be taken into account. First, a correction is applied to account for the kinematic and geometrical acceptances of the muons in the muon control sample. It is determined by applying a muon smearing procedure to events in W and $t\bar{t}$ simulated samples with a W-decay muon passing the muon kinematic selection, and comparing the resulting event yield to the one obtained using all muons from W decays in the same event samples. A second correction takes into account the muon trigger, reconstruction and isolation efficiencies. The same procedure as described in Section 5.1 is followed, parametrizing the identification

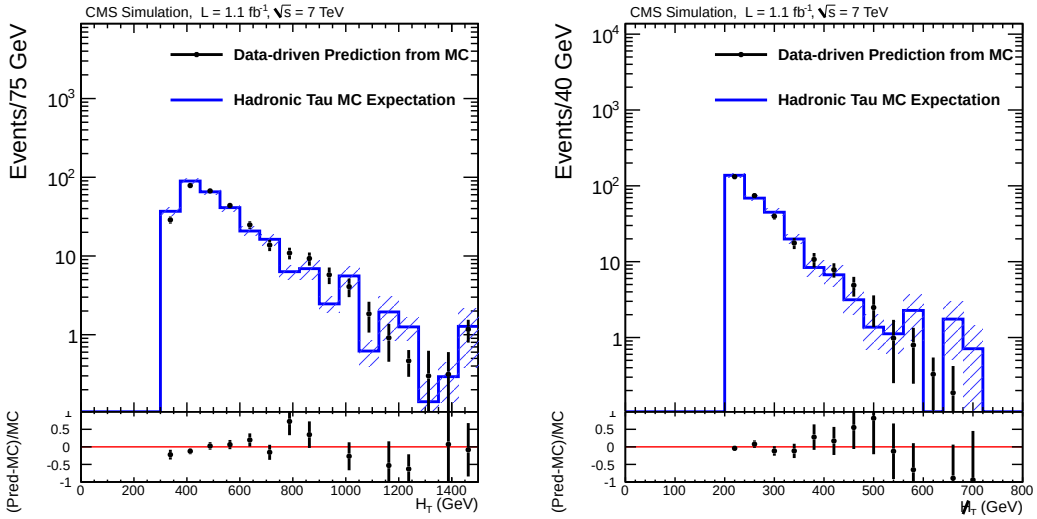

Figure 5: The closure test of the method for the hadronic-τ background prediction. H_T (left) and $\not{H}_T$ (right) distributions predicted from simulated events using the data-driven method compared to the MC expectation of the hadronic-τ background for the baseline selection. Uncertainties are statistical only. The fractional difference of the data-driven prediction from simulated events with respect to the MC expectation is also shown.

efficiency as a function of ${p_T}^{\mu}$ and η^{μ}, and isolation efficiency as a function of ${p_T}^{\text{nearest jet}}/{p_T}^{\mu}$ and $\Delta R(\mu, \text{nearest jet})$. A correction is also applied for the relative branching fractions for W decays into muon or hadronic-τ jets.

The above procedure for predicting the hadronic-τ background is tested on simulated W and $t\bar{t}$ events and reproduces the expectation from the simulation of true hadronic taus from W and $t\bar{t}$ within uncertainties. The evaluation of the statistical uncertainty on the prediction needs special attention due to the multiple sampling of the response template. This uncertainty is evaluated with a set of pseudo-experiments using a so-called bootstrap technique [51].

All considered systematic uncertainties and their impact on the prediction are summarized in Table 6. The possible discrepancy between data and simulation for the τ energy template is taken into account as a systematic uncertainty estimated by scaling the visible energy fraction by 3% [52]. $Z \to \mu^+\mu^-$, $t\bar{t}/W+X \to \tau\nu+X \to \mu\nu+X$, and the QCD multijet events contribution is measured using MC simulation and subtracted. A conservative 50% uncertainty is assigned to this subtraction.

The number of $W/t\bar{t} \to \tau_h+X$ events predicted in data using this method is summarized in Table 7 for the different signal regions.

Table 6: Systematic uncertainties for the hadronic-τ background prediction for each of the selections. SM subtraction refers to the MC standard model processes which are subtracted.

Type of the effect (in %)	Baseline	Medium	High H_T	High $\not{H}_T$
τ energy scale	-1.8, $+1.5$	-2.3, $+1.1$	-1.9, $+1.7$	-0.0, $+0.0$
Acceptance	-1.6,$+1.6$	-1.7,$+1.7$	-2.3,$+2.3$	-2.6,$+1.8$
Muon ID, ISO and Trigger	± 0.1	± 0.3	± 0.3	± 1.0
SM Subtraction	± 2.3	± 3.6	± 2.4	± 6.1

Table 7: The W and $t\bar{t}$ hadronic-τ background predicted for each of the selections with the statistical and systematic uncertainties. The prediction corresponds to 1.1 fb^{-1}.

	Baseline			Medium			High H_T			High $\not{H}_T$		
Prediction	263	± 8	± 7	17	± 2	± 0.7	18	± 2	± 0.5	0.73	± 0.73	± 0.04

6 QCD Background Estimation

QCD multijet production is a difficult background to predict in all-hadronic new-physics searches, because the tails of distributions require a precise detector simulation, while theoretical models may exhibit large uncertainties.

A data-driven technique is used to estimate the multijet background from first principles, called the Rebalance and Smear (R+S) method. This method predicts the full kinematics in multijet events from data, while being unaffected by the potential presence of signal. The R+S method is presented in more detail in Sections 6.1 and 6.3. A crucial input to this methodology are the jet energy resolutions, for which the measurement from data including the non-Gaussian tails [32] is described in Section 6.2.

6.1 The Rebalance+Smear method

6.1.1 Concepts of the Rebalance+Smear QCD multijet prediction

High $\not{H}_T$ arises in QCD multijet events from jet energy mismeasurements, in particular when one or more jets in the event have a jet energy response far from unity, where this response reflects the correspondence between reconstructed jets and particle jets at the generator level. The R+S method to predict the QCD multijet background is essentially a simplified simulation where the jet response is modelled by a parametrized function, and where instead of generated jets we use a sample of "seed events" obtained from data consisting of "seed jets" that are good estimators of the true QCD particle-jet momenta.

The seed events are produced in the "Rebalance" step using an inclusive multijet data sample as input. All of the jet momenta are adjusted in a manner consistent with expected measurement uncertainties to return the event back into approximate transverse momentum balance. This forces events with true high $\not{H}_T$ from neutrinos or other undetected particles into well balanced QCD-like events. As such $t\bar{t}$, W+jets, and Z+jets events, but also contributions from new physics, if any, have negligible impact on the background prediction as their production rate is much smaller than the QCD multijet production rate.

In the "Smear" step the momentum of each seed jet is scaled by a factor drawn from the jet response distribution in order to model the expected reconstructed momentum. As the seed events are representative of a pure QCD multijet sample, the resulting events can be used to apply search cuts while maintaining the prediction of all event-by-event jet kinematics. This allows for great flexibility in the set of variables that can be used to either define a search region, or to eventually characterize some observed new physics signal.

Since the search cuts include large values of $\not{H}_T$ only a few smeared events will enter the search region. In order to get the most accurate prediction we use the bootstrap method [51], repeating the method many times and use the mean of the ensemble of predictions as the central prediction and the variance as a statistical uncertainty.

6.1.2 Parametrized jet resolution functions

The response functions are determined from simulated PYTHIA QCD dijet samples and are modified to match the measurement from the data as described in Section 6.2.1. The jet response parametrization employed in the R+S method depends on properties of the particle jet itself. Because of the improving CMS calorimeter resolution for more energetic jets, the Gaussian core of the response improves with increasing energy. The contributions of various components in the non-Gaussian response tails also exhibit an energy dependence, such as the rising loss of high p_T hadrons that "punch-through" the calorimeters. Therefore, the jet responses are parametrized in p_T and η.

6.1.3 Rebalancing

Balanced events that serve as input to the smearing step are constructed in the R+S method by adjusting ("rebalancing") the jet momenta. This leads to an $\not{H}_T$ estimator after smearing that is robust against jet mismeasurements.

Good estimators for the particle jet momenta can be obtained by a kinematic fit subject to the transverse momentum balance constraint; in the kinematic fit the p_T, η and ϕ of the measured jets are adjusted to fulfill the constraints and minimize a χ^2 calculated from the squared residuals of measured and fitted jets. To reduce the effect of pileup which produces high numbers of jets at low p_T, only jets above a threshold of $p_T > 10\,\text{GeV}$ are considered during the fit. Since the rebalance step was observed to be insensitive to tails in the response functions, only the Gaussian core resolution is further used to rebalance the events.

6.1.4 Performance in Monte-Carlo Simulation

The performance of the R+S procedure is demonstrated using fully simulated PYTHIA QCD multijet samples including pileup interactions. The response functions are derived from the same samples. Seed events are preselected to have at least two seed jets with $p_{T,\text{min}}^{\text{seed}} > 50\,\text{GeV}$. This selection is chosen to be sufficiently loose compared to the requirements in the search regions of three jets and $H_T > 350\,\text{GeV}$.

In Fig. 6 the predicted H_T and $\not{H}_T$ distributions are shown and compared to fully simulated data, and the results are summarized in Table 8. For a loose selection of three jets with $p_T > 50\,\text{GeV}$ and $|\eta| < 2.5$, the level of closure for H_T is within 10%. The $\not{H}_T$ distribution for events passing in addition $H_T \geq 350\,\text{GeV}$ and $\Delta\phi(\not{H}_T, \text{jet 1-3})$, is more sensitive to the jet response definition and parametrization, with closure within 10% up to $\not{H}_T$ values of 200 GeV; above 200 GeV the agreement of the R+S prediction and full simulation is within the statistical uncertainties. As a further check the prediction was done without the cut on $\Delta\phi(\not{H}_T, \text{jet 1-3})$, and shows a good agreement up to high $\not{H}_T$ values. For the different search regions the ratio of fully simulated events and the R+S prediction is used as a bias correction factor. Since the statistical uncertainties for high $\not{H}_T$ selections are large, for $\not{H}_T > 350\,\text{GeV}$ and $> 500\,\text{GeV}$ no bias correction is applied.

6.2 Jet energy response measurements

The R+S method relies on the jet momentum resolution. For the rebalancing of the event, it is sufficient to use the Gaussian core of the response distribution (resolution) but for smearing, and therefore the prediction of the $\not{H}_T$ spectrum, the full distribution including the non-Gaussian tails have to be known. The jet momentum response was measured from QCD dijet events. They were collected by triggering on p_T^{ave}, the average p_T of the leading two jets in an event, and sorted in bins of p_T^{ave}. By comparison of the results in data and MC simulation,

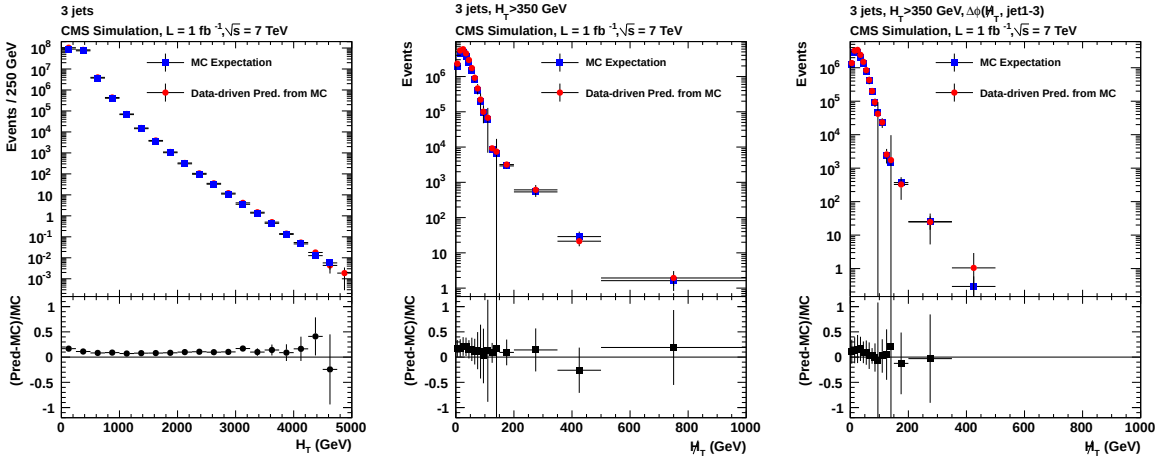

Figure 6: R+S prediction compared to fully simulated MC distributions. Left: H_T distribution for events passing $\geq$ 3 jets; middle: $\not{H}_T$ distribution for events passing $\geq$ 3 jets and $H_T \geq$ 350 GeV; right: $\not{H}_T$ distribution for events passing $\geq$ 3 jets, $H_T \geq$ 350 GeV, and $\Delta\phi(\not{H}_T, \text{jet 1-3})$.

Table 8: Number of events predicted to pass various event selections for 1 fb^{-1} of integrated luminosity, for the fully simulated PYTHIA QCD sample and for the R+S prediction when executed on this same MC sample (statistical uncertainties only). The last row is the ratio of the MC over R+S predicted yields. Since the mean of ensemble of R+S prediction has a much smaller uncertainty, the error on the ratio is calculated from the statistical error of the full simulation only.

	No $\Delta\phi$ cuts	Baseline	$H_T > 500$ GeV	$H_T > 800$ GeV
N(PYTHIA)	565 ± 37	25.7 ± 10.9	25.7 ± 10.9	12.1 ± 3.6
N(R+S)	634 ± 225	25.8 ± 19.5	20.5 ± 14.8	10.6 ± 6.2
N(PYTHIA)/N(R+S)	0.89 ± 0.06	1.00 ± 0.42	1.25 ± 0.53	1.13 ± 0.34

correction factors to the MC truth response were derived. The measurement was performed in two steps: First, correction factors to the core resolution were measured using a maximum likelihood method. Then, tail correction factors were derived by comparing the tails of the dijet asymmetry distributions in data and simulation.

6.2.1 Gaussian resolution

The Gaussian resolution was measured using an unbinned maximum likelihood method based on the transverse momentum balance at parton level in QCD dijet events. In order to correct for selection biases, the shape of the underlying particle level jet p_T spectrum was taken into account.

Additional jets in the event due to soft radiation break the momentum balance between the two leading jets at particle level. Hence, the resolution was determined for different thresholds on the p_T of the third leading jet and extrapolated to zero additional jet activity by a straight line fit, Fig. 7 (left). A further, small correction for out-of-cone showering and hadronization effects was taken from the Monte Carlo simulation. The resolution was measured in the central η region to be $\sim$ 5% larger in data compared to the Monte Carlo simulation, increasing up to $\sim$ 30% in the very forward region. No significant dependence of this difference on the p_T of the jet has been observed. Therefore, correction factors were finally obtained as the ratio of the resolutions measured in data and simulation, averaged in p_T for different pseudorapidity

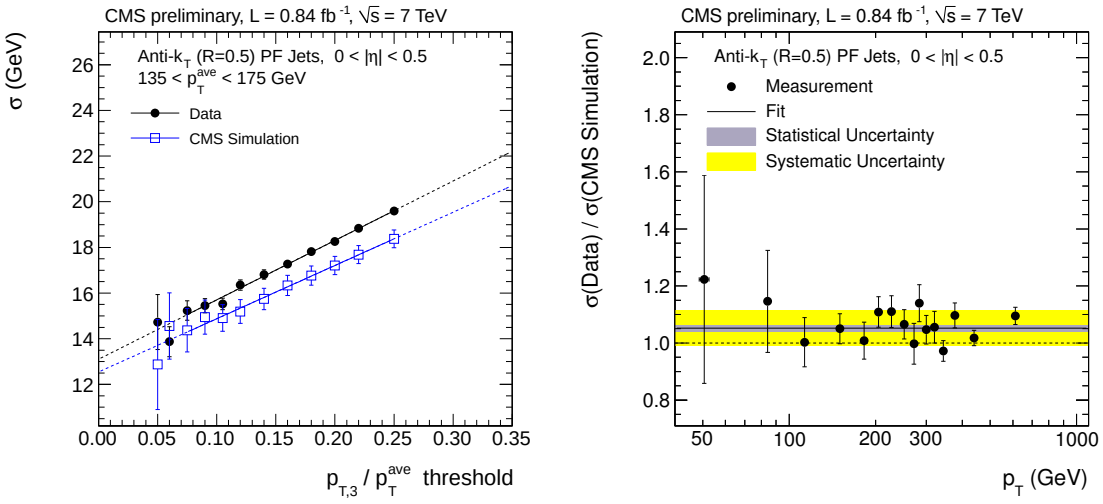

Figure 7: (Left) The jet p_{T} resolution as a function of the threshold on $p_{\mathrm{T}}^{3\mathrm{rd}}/p_{\mathrm{T}}^{\mathrm{ave}}$ for one example bin in $p_{\mathrm{T}}^{\mathrm{ave}}$ and η. The results from simulation (open squares) are overlaid with the measurement from data (solid circles). They are fitted with a straight line to extrapolate to zero additional jet activity. (Right) Ratio of the extrapolated resolution measured in data and simulation in the central η bin as a function of p_{T}. The correction factor is obtained by fitting a constant.

intervals, Fig. 7 (right). The factors are applied by a convolution of the MC truth response with an appropriate Gaussian.

Since the correction factors are measured in terms of a data to Monte Carlo ratio, common biases and correlated systematic uncertainties cancel. The remaining systematic uncertainty is dominated by the uncertainties on the jet energy scale and the extrapolation method, and amounts to $\sim 5\%$ in the central η region, and increases up to $\sim 20\%$ in the very forward region.

6.2.2 Non-Gaussian tails

The tails of the jet response function are of particular importance to the prediction of the QCD multijet background at high $\not{H}_{\mathrm{T}}$. As for the core resolution, correction factors to the tails of the MC truth response function were measured from data.

Here, the dijet asymmetry, $(p_{\mathrm{T},1} - p_{\mathrm{T},2})/(p_{\mathrm{T},1} + p_{\mathrm{T},2})$ with randomly ordered leading jets, was used. The number of events with large asymmetries in data and Monte Carlo simulation was compared. Since the core resolution, and thus the width of the asymmetry distribution, differ between data and Monte Carlo simulation, the simulated asymmetry distribution was first adjusted to fit the data. It was then used to define a tail region, as shown in the left hand side of Fig. 8. Similar to the case of the core resolution measurement, the dependence of the fractional number of events in this tail region on the dijet selection threshold $p_{\mathrm{T}}^{3\mathrm{rd}}$ was extrapolated to the ideal dijet topology. Scale factors to the response tails were derived from the ratio of the extrapolated fractional number of events in data and simulation; the result for one $p_{\mathrm{T}}^{\mathrm{ave}}$ and η bin is shown in Fig. 8 (right).

Different tail regions in asymmetry were used to test the stability of the method and check for possible shape differences in the response distributions in simulation and data. Within the statistical uncertainties, no such dependence was observed. The dominant systematic uncertainty originates in the correction of the Gaussian core difference between data and Monte Carlo simulation, which is propagated to the result. Moreover, uncertainties due to the extrapolation

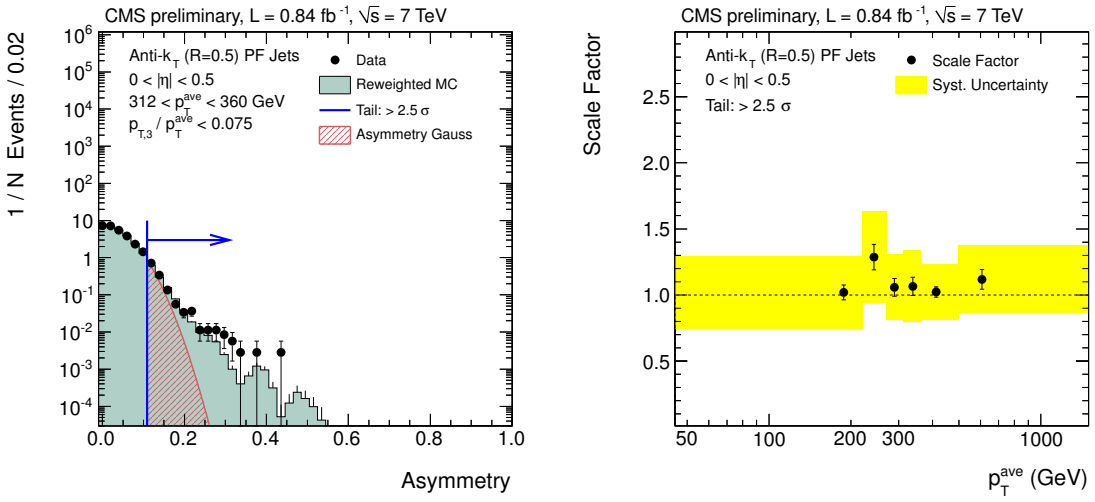

Figure 8: (Left) Example dijet asymmetry distribution for data (solid circles) compared to the Monte Carlo simulation (filled histogram). The latter has been corrected for the measured core resolution differences. The area beyond asymmetries of 0.1, indicated by the arrow, defines the tail region. For comparison, the hatched area shows number of events expected for a purely Gaussian response. (Right) Ratios of the fractional number of tail events in data and MC simulation in bins of $p_{\mathrm{T}}^{\mathrm{ave}}$ for the central η region. They were used as scale factors for the tails of the MC truth response distribution.

procedure, pileup effects, and the residual non-closure of the method were evaluated. In total, they amount to $\sim$ 25% in the central η region and increase up to 40% in the very forward region.

The MC truth jet response was corrected by scaling the non Gaussian parts of the response distribution by the measured scale factors. However, no significant deviation of the simulated jet response tails from data has been observed.

6.3 Results of the Rebalance+Smear method

For the data set used in this analysis the high instantaneous luminosity requires the signal trigger to be an H_{T}-$\not{H}_{\mathrm{T}}$ cross trigger. The R+S method uses as input events which are collected with an H_{T} trigger with no additional $\not{H}_{\mathrm{T}}$ requirement, providing in this way an unbiased seed sample. Since the lowest unprescaled H_{T} triggers have thresholds of 500 GeV or more, the seed sample has to be obtained by combining several H_{T} triggers down to a threshold of 150 GeV, taking into account their prescales. The inclusion of prescaled events leads to increased statistical uncertainties for the R+S method, because of single events with large weights.

To predict the QCD multijet background in the baseline and search regions the R+S method is carried out using the inclusive data sample, and fulfilling the preselection of two jets with $p_{\mathrm{T}} > 50\,\mathrm{GeV}$.

The rebalance and smear steps are then executed using Monte Carlo Truth jet energy response functions with applied correction factors for the Gaussian core resolution and the non-Gaussian tails from Section 6.2. The background predictions are finally obtained by applying the event selection requirements on the rebalanced and smeared events.

In Table 9 the number of predicted events is listed for the baseline and search regions, along with the considered systematic uncertainties.

Table 9: The QCD multijet background predicted for each of the selections along with all considered uncertainties. The prediction corresponds to 1.1 fb^{-1}.

	Baseline	Medium	High H_T	High $\not{H}_T$
Bias-corrected prediction	31	1.3	13.5	0.09
Seed sample statistics	$\pm$114%	$\pm$102%	$\pm$30%	$\pm$340%
Resolution core	$^{+10\%}_{-8\%}$	$^{+3\%}_{-8\%}$	$^{+9\%}_{-9\%}$	$^{+1\%}_{-18\%}$
Resolution tail	$^{+31\%}_{-19\%}$	$^{+17\%}_{-34\%}$	$^{+33\%}_{-31\%}$	$^{+41\%}_{-36\%}$
Flavour trend	$\pm$10%	$\pm$10%	$\pm$10%	$\pm$10%
R+S non-closure	$\pm$40%	$\pm$40%	$\pm$40%	$\pm$40%
Pileup effects	$\pm$10%	$\pm$10%	$\pm$10%	$\pm$10%
Total uncertainty	$^{+125\%}_{-116\%}$	$^{+112\%}_{-107\%}$	$^{+62\%}_{-44\%}$	$^{+347\%}_{-345\%}$

6.3.1 Systematic uncertainties

Several uncertainties are taken into account. First of all, a statistical uncertainty is associated to the size of the seed event sample. As prescribed by the bootstrap method, an ensemble of pseudo-datasets are created by sampling with replacement from the original seed sample. The ensemble variance of predictions made from these pseudo-datasets is taken as the statistical uncertainty.

Because of several effects the data-driven prediction is expected to be biased: Incompleteness in the jet resolution parametrization can be evaluated by smearing of generator level jets. Depending on the tested selections, the predictions deviate by 10% to 20% from the full simulation. Another bias arises from neglecting jets below the threshold in the rebalancing procedure ($< 10\%$), and a third small bias ($< 5\%$) from migration effects of the steeply falling jet spectrum and the finite resolution. Since in the presence of pileup, the bias due to the jet p_T cut is difficult to disentangle from the other effects, an overall correction factor is derived from Monte Carlo closure tests ($< 25\%$). In total we assign a systematic uncertainty of 40% (box distribution) from these sources.

Another large systematic effect arises from the jet response knowledge. The measurement uncertainties discussed in Sections 6.2.1 and 6.2.2 on the core resolutions and non-Gaussian tails are propagated by repeating the R+S prediction with the $\pm 1\sigma$ varied inputs. The corresponding uncertainties are asymmetric and the corresponding underlying distributions are assumed to be of two truncated Gaussians.

The Monte Carlo response templates are obtained from PYTHIA and thus implicitly use the heavy flavour content as implemented in the PYTHIA generator. Previous studies [19] have shown that for moderate $\not{H}_T$ cuts the uncertainty is $< 10\%$ (normal distributed).

The trigger selection of the seed sample is done in such a way as to be unbiased in $\not{H}_T$ and having events down to values below the H_T threshold of the signal trigger. This needs the usage of prescaled triggers, which get sometimes large weights and therefore increase the statistical uncertainties. Apart from this, no bias is introduced by the triggers.

A final effect to take into account is the presence of pileup collisions. Neglecting jets below this threshold makes the current implementation safe against pileup effects. To study possible residual effects, the MC was reweighted according to the observed pileup distribution in data, and the mean of this distribution was shifted by ± 1. In the search regions the uncertain-

ties are dominated by the statistical errors of the used Monte Carlo sample and no significant pileup dependence has been observed. However, a conservative uncertainty of 10% (normal distributed) is assumed, which are the obtained fluctuations for the pileup variations. To check the R+S prediction from data we determined the dependence on the number of pileup events; no such dependence has been observed.

7 Results and Interpretation

The predicted event yields from the different data-driven background estimation methods discussed in the previous sections and the number of events observed in 1.1 fb^{-1} of data are summarized in Table 10 for the baseline and three search selections. Figure 9 also shows the H_T and $\not{H}_T$ distributions for the combined data-driven background predictions for the baseline selection, together with those observed in data. For the combination of all the data-driven background estimates, the probability distributions corresponding to each uncertainty source, whether Gaussian, bifurcated Gaussian, Poisson or box shaped, are convoluted together by numerical integration using Monte-Carlo techniques to obtain the probability distributions for each background and for the overall background estimation. The resulting distribution is fitted to a Gaussian function, as expected from the Central Limit Theorem, and the mean and sigma are used as the central value and uncertainty in the limit calculations. This procedure results in a combined background which is very close but not identical to the linear sum of the backgrounds. Some differences are observed between the data-driven estimates of SM background and expectations from MC simulation, as shown in Tables 10 and 1, indicating the importance of the data-driven background estimation.

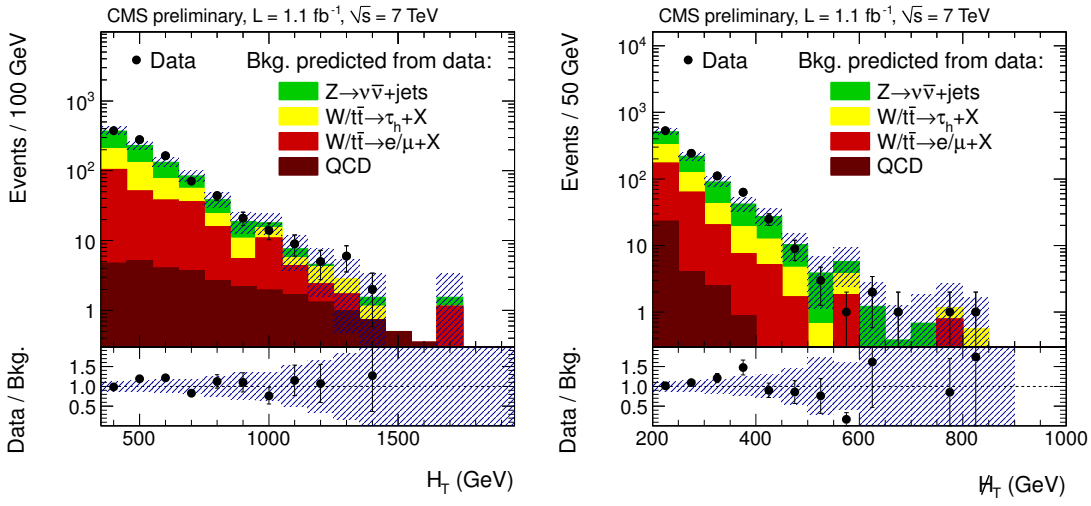

Figure 9: H_T (left) and $\not{H}_T$ (right) distributions in data compared to the combined data-driven background predictions. The ratio of data to the combined data-driven background predictions is also shown. While the integrated background uncertainty corresponds to the values listed in Table 10, the bin-by-bin combination of the background contributions and their uncertainties has been performed in a simplified way assuming Gaussian probability distributions.

No significant excess of events is observed in any of the search regions compared to the SM background estimates.

In the absence of an observed signal, limits are set on the parameter space of the CMSSM. In Fig. 10 the observed and expected CLs [53, 54] exclusion limits at the 95% confidence level are

Table 10: Predicted event yields from the different background estimation methods for the baseline selection and for the search selections. The total background estimates are calculated as described in the text.

	Baseline (H_T >350 GeV) ($\not{H}_T$ >200 GeV)	Medium (H_T >500 GeV) ($\not{H}_T$ >350 GeV)	High H_T (H_T >800 GeV) ($\not{H}_T$ >200 GeV)	High $\not{H}_T$ (H_T >800 GeV) ($\not{H}_T$ >500 GeV)
$Z \to \nu\bar{\nu}$ from γ+jets	$376 \pm 12 \pm 79$	$42.6 \pm 4.4 \pm 8.9$	$24.9 \pm 3.5 \pm 5.2$	$2.4 \pm 1.1 \pm 0.5$
$t\bar{t}/W \to e, \mu$+X	$244 \pm 20^{+30}_{-31}$	$12.7 \pm 3.3 \pm 1.5$	$22.5 \pm 6.7^{+3.0}_{-3.1}$	$0.8 \pm 0.8 \pm 0.1$
$t\bar{t}/W \to \tau_h$+X	$263 \pm 8 \pm 7$	$17 \pm 2 \pm 0.7$	$18 \pm 2 \pm 0.5$	$0.73 \pm 0.73 \pm 0.04$
QCD	$31 \pm 35^{+17}_{-6}$	$1.3 \pm 1.3^{+0.6}_{-0.4}$	$13.5 \pm 4.1^{+7.3}_{-4.3}$	$0.09 \pm 0.31^{+0.05}_{-0.04}$
Total background	928 ± 103	73.9 ± 11.9	79.4 ± 12.2	4.6 ± 1.5
Observed in data	986	78	70	3

shown in the CMSSM m_0-$m_{1/2}$ plane for $\tan\beta = 10$, $\mu > 0$, and $A_0 = 0$ using the NLO signal cross section, obtained with the program PROSPINO [44]. The shown contours are based on the combination of limits from all three search regions used in this search, i.e. the most stringent limit from three search regions is used to determine the exclusion. At low m_0 the observed exclusion reaches the values of the common gaugino mass at the GUT scale $m_{1/2}$ of 530 GeV, and at $m_0 = 1500$ GeV the exclusion reaches $m_{1/2}$ of 230 GeV, significantly extending the m_0-$m_{1/2}$ exclusion results from a similar search using the data collected in 2010 [19]. The exclusion limits are similar to those obtained by the 2011 CMS search using the α_T kinematic variable [20].

8 Conclusions

An inclusive search for new physics was presented using events with a multijet signature with large missing transverse momentum collected in proton–proton collisions at $\sqrt{s} = 7$ TeV with the CMS detector at the LHC. The data sample corresponds to an integrated luminosity of $1.1\,\text{fb}^{-1}$. This search presents an update of the analysis reported in [19]. The observed event yield is consistent with the standard-model background contributions mainly arising from invisible Z+jets, W+jets, $t\bar{t}$ and QCD multijet production. These SM contributions were estimated from the data using techniques which result in a minimal reliance on simulation. In the absence of a significant excess of events above the SM background expectation, exclusion limits were established at the 95% confidence level in the CMSSM phase space, which exceed those set by previous searches. At low m_0 and $m_0 = 1500$ GeV the exclusion reaches $m_{1/2} = 530$ and 230 GeV, respectively.

References

[1] J. Wess and B. Zumino, "Supergauge transformations in four dimensions", *Nucl. Phys.* **B70** (1974) 39.

[2] H.-C. Cheng and I. Low, "TeV symmetry and the little hierarchy problem", *JHEP* **0309** (2003) 051, arXiv:hep-ph/0308199.

[3] T. Appelquist, H.-C. Cheng, and B. A. Dobrescu, "Bounds on universal extra dimensions", *Phys. Rev.* **D 64** (2001) 035002, arXiv:hep-ph/0012100. doi:10.1103/PhysRevD.64.035002.

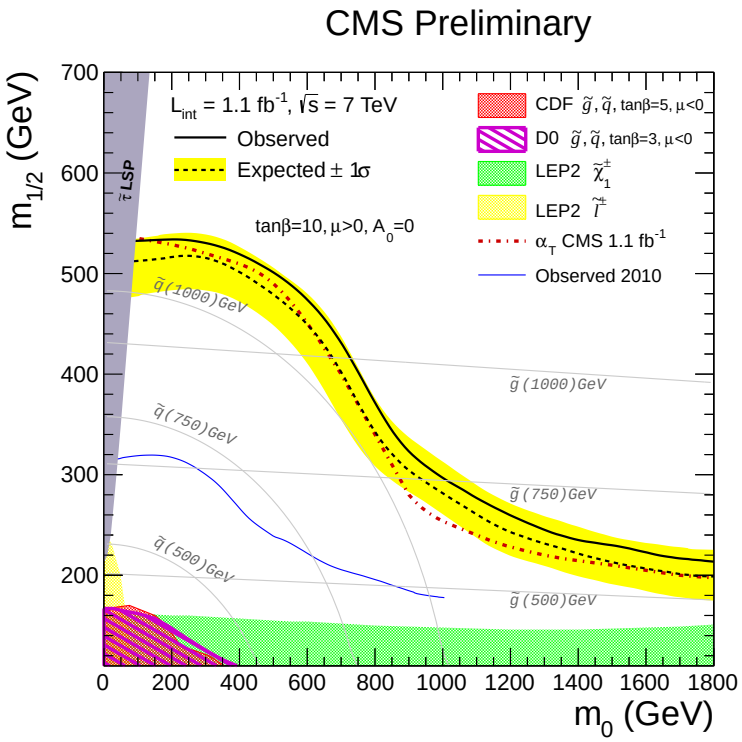

Figure 10: The observed and expected 95% CL exclusion contours in the CMSSM parameter m_0-$m_{1/2}$ plane using the signal cross sections calculated at NLO. The shown contours are the combination of the different selections, such that the shown contours are the envelope with respect to the best sensitivity. The remaining CMSSM parameters are $\tan\beta = 10$, $\mu > 0$, and $A_0 = 0$. The limits from earlier CMS searches and from other experiments are also shown.

[4] J. L. Feng, "Dark Matter Candidates from Particle Physics and Methods of Detection", arXiv:1003.0904.

[5] CDF Collaboration, Altonen et al., "The CDF exclusion region in the $m_{1/2}$ vs. m_0 plane", *Phys. Rev. Lett* **102** (2009) 121801, arXiv:011.2512.

[6] D0 Collaboration, Abazov et al., "Search for squarks and gluinos in events with jets and missing transverse energy using 2.1 fb^{-1} of $p\bar{p}$ collision data at $\sqrt{s} = 1.96$ TeV", *Phys. Lett.* **B 660** (2008) 449, arXiv:0712.3805.

[7] D0 Collaboration, "Search for associated production of charginos and neutralinos in the trilepton final state using 2.3 fb^{-1} of data", *Phys. Lett.* **B 680** (2009), no. 1, 34 – 43. doi:DOI: 10.1016/j.physletb.2009.08.011.

[8] UA1 Collaboration, C. Albajar et al., "Events with Large Missing Transverse Energy at the CERN Collider 3: Mass Limits on Supersymmetric Particles", *Phys. Lett.* **B 198** (1987) 261.

[9] UA2 Collaboration, R. Ansari et al., "Search For Exotic Processes at the CERN $p\bar{p}$ Collider", *Phys. Lett.* **B 195** (1987) 613.

[10] ALEPH Collaboration, "Absolute Mass Lower Limit for the Lightest Neutralino of the MSSM from e^+e^- data at $\sqrt{s}$ up to 209 GeV", *Phys. Lett.* **B 583** (2004) 247. See also references therein. doi:10.1016/j.physletb.2003.12.066.

[11] DELPHI Collaboration, "Searches for Supersymmetric Particles in e^+e^- Collisions up to 208 GeV and Interpretation of the Results within the MSSM", *Eur. Phys. J. C* **31** (2003) 421, arXiv:hep-ex/0311019. See also references therein. doi:10.1140/epjc/s2003-01355-5.

[12] L3 Collaboration, "Search for Scalar Leptons and Scalar Quarks at LEP", *Phys. Lett.* **B 580** (2004) 37, arXiv:hep-ex/0310007. See also references therein. doi:10.1016/j.physletb.2003.10.010.

[13] OPAL Collaboration, "Search for Chargino and Neutralino Production at $\sqrt{s} = 192$ GeV to 209 GeV at LEP", *Eur. Phys. J. C* **35** (2004) 1, arXiv:hep-ex/0401026. See also references therein. doi:10.1140/epjc/s2004-01780-x.

[14] ZEUS Collaboration, "Search for Stop Production in R-Parity-Violating Supersymmetry at HERA", *Eur. Phys. J. C* **50** (2007) 269, arXiv:hep-ex/0611018. doi:10.1140/epjc/s10052-007-0240-8.

[15] H1 Collaboration, "A Search for Selectrons and Squarks at HERA", *Phys. Lett.* **B 380** (1996) 461, arXiv:hep-ex/9605002. doi:10.1016/0370-2693(96)00640-5.

[16] L. Randall and D. Tucker-Smith, "Dijet Searches for Supersymmetry at the LHC", *Phys. Rev. Lett.* **101 221803** (2008).

[17] CMS Collaboration, "Search for Supersymmetry in pp Collisions at 7 TeV in Events with Jets and Missing Transverse Energy", *Phys. Lett.* **B 698** (2011) 196–218, arXiv:1101.1628. doi:10.1016/j.physletb.2011.03.021.

[18] CMS Collaboration, "Inclusive search for squarks and gluinos in pp collisions at $\sqrt{s} = 7$ TeV", arXiv:1107.1279.

[19] CMS Collaboration, "Search for New Physics with Jets and Missing Transverse Momentum in pp collisions at $\sqrt{s} = 7$ TeV", arXiv:1106.4503.

[20] CMS Collaboration, "Search for Supersymmetry in pp Collisions at 7 TeV in Events with Jets and Missing Transverse Energy", *CMS-PAS-SUS-11-003* (2011).

[21] C. G. Lester and D. J. Summers, "Measuring masses of semi-invisibly decaying particles pair produced at hadron colliders", *Phys. Lett.* **B 463** (1999) 99–103, arXiv:hep-ph/9906349. doi:10.1016/S0370-2693(99)00945-4.

[22] A. Barr, C. Lester, and P. Stephens, "m_{T2}: the Truth behind the glamour", *J. Phys. G* **29** (2003) 2343–2363, arXiv:hep-ph/0304226. doi:10.1088/0954-3899/29/10/304.

[23] CMS Collaboration, "Search for supersymmetry in hadronic final states using M_{T2} in 7 TeV pp collisions at the LHC", *CMS-PAS-SUS-11-005* (2011).

[24] ATLAS Collaboration, "Search for squarks and gluinos using final states with jets and missing transverse momentum with the ATLAS detector in $\sqrt{s} = 7$ TeV proton-proton collisions", *Phys. Lett.* **B 701** (2011) 186–203, arXiv:1102.5290. doi:10.1016/j.physletb.2011.05.061.

[25] ATLAS Collaboration, "Search for squarks and gluinos using final states with jets and missing transverse momentum with the ATLAS detector in 7 TeV proton-proton collisions", *ATLAS-CONF-2011-086* (2011).

[26] A. H. Chamseddine, R. L. Arnowitt, and P. Nath, "Locally Supersymmetric Grand Unification", *Phys. Rev. Lett.* **49** (1982) 970. doi:10.1103/PhysRevLett.49.970.

[27] R. L. Arnowitt and P. Nath, "SUSY Mass Spectrum in SU(5) Supergravity Grand Unification", *Phys. Rev. Lett.* **69** (1992) 725. doi:10.1103/PhysRevLett.69.725.

[28] G. L. Kane, C. Kolda, L. Roszkowski and J. D. Wells, "Study of constrained minimal supersymmetry", *Phys. Rev.* **D 49** (1994) 6173–6210.

[29] CMS Collaboration, "The CMS experiment at the CERN LHC", *JINST* **0803** (2008) S08004.

[30] CMS Collaboration, "Particle Flow Event Reconstruction in CMS and Performance for Jets, Taus and MET", *CMS-PAS-PFT-09-001* (2009).

[31] M. Cacciari, G. P. Salam, and G. Soyez, "The anti-kt jet clustering algorithm", *JHEP* **0804:063** (2008).

[32] CMS Collaboration, "Determination of Jet Energy Calibration and Transverse Momentum Resolution in CMS", arXiv:1107.4277.

[33] M. Cacciari and G. P. Salam, "Pileup subtraction using jet areas", *Phys. Lett.* **B 659** (2007) 119. doi:10.1016/j.physletb.2007.09.077.

[34] M. Cacciari, G. P. Salam, and G. Soyez, "The Catchment Area of Jets", *JHEP* **04** (2007) 005. doi:10.1088/1126-6708/2008/04/005.

[35] CMS Collaboration, "HCAL performance from first collisions data", *CMS-DPS-2010-025* (2010).

[36] CMS Collaboration, "Missing transverse energy performance of the CMS detector", arXiv:1106.5048.

[37] CMS Collaboration, "Electromagnetic calorimeter commissioning and first results with 7 TeV data", *CMS-NOTE-2010-012* (2010).

[38] J. Allison et al., "Geant4 - developments and applications", *IEEE 53* **1** (2006) 270–278.

[39] T. Sjöstrand, S. Mrenna, and P. Z. Skands, "PYTHIA 6.4 Physics and Manual", *JHEP* **05** (2006) 026, arXiv:hep-ph/0603175.

[40] J. Alwall et al., "MadGraph/MadEvent v4: The New Web Generation", *JHEP* **09** (2007) 028, arXiv:0706.2334.

[41] N. Kidonakis, "Next-to-next-to-leading Soft-Gluon Corrections for the Top Quark Cross Section and Transverse Momentum Distribution", *Phys. Rev.* **D 82** (2010) 114030, arXiv:1009.4935. doi:10.1103/PhysRevD.82.114030.

[42] K. Melnikov and F. Petriello, "Electroweak Gauge Boson Production at Hadron Colliders through $O(\alpha(s)^2)$", *Phys. Rev.* **D 74** (2006) 114017, arXiv:hep-ph/0609070. doi:10.1103/PhysRevD.74.114017.

[43] CMS Collaboration, "CMS Technical Design Report, Volume II: Physics Performance", *J. Phys. G* **34** (2007) 995.

[44] W. Beenakker, R. Hopker, and M. Spira, "PROSPINO: A program for the PROduction of Supersymmetric Particles In Next-to-leading Order QCD", arXiv:hep-ph/9611232.

[45] CMS Collaboration, "Isolated Photon Reconstruction and Identification at $\sqrt{s} = 7$ TeV", *CMS-PAS-EGM-10-006* (2010).

[46] P. Aurenche, M. Fontannaz, J.-P. Guillet et al., "A New critical study of photon production in hadronic collisions", *Phys. Rev.* **D 73** (2006) 094007, arXiv:hep-ph/0602133.

[47] CMS Collaboration, V. Khachatryan et al., "Measurement of the Isolated Prompt Photon Production Cross Section in pp Collisions at sqrt(s) = 7 TeV", *Phys. Rev. Lett.* **106** (2011) 082001, arXiv:1012.0799.

[48] CMS Collaboration, "Measurement of the Differential Isolated Prompt Photon Production Cross Section in pp Collisions at $\sqrt{s} = 7$TeV", *CMS-PAS-QCD-10-037, in preparation* (2011).

[49] Z. Bern et al. (BlackHat collaboration), private communication(s) and to appear.

[50] J. H. Kuhn, A. Kulesza, S. Pozzorini et al., "Electroweak corrections to hadronic photon production at large transverse momenta", *JHEP* **03** (2006) 059, arXiv:hep-ph/0508253. doi:10.1088/1126-6708/2006/03/059.

[51] B. Efron, "The Jackknife, The Bootstrap and Other Resampling Plans", volume 38 of *CBMS-NSF Regional Conference Series in Applied Mathematics*. SIAM, Philadelphia, 1982.

[52] CMS Collaboration, "Tau Identification in CMS", *CMS-PAS-TAU-11-001* (2011).

[53] A. Read, "Presentation of search results: the CLs technique", *Journal of Physics G: Nucl. Part. Phys.* **28** (2002) 2693–2704.

[54] T. Junk, "Confidence level computation for combining searches with small statistics", *Nuclear Instruments and Methods* **A434** (1999) 435–443.